Scanning Kelvin probe microscopy of surface electronic structure in GaN grown by hydride vapor phase epitaxy

B. S. Simpkins, D. M. Schaadt, and E. T. Yu[a)]
Department of Electrical and Computer Engineering and Program in Materials Science and Engineering, University of California at San Diego, La Jolla, California 92093-0407

R. J. Molnar
Lincoln Laboratory, Massachusetts Institute of Technology, Lexington, Massachusetts 02420-9108

(Received 28 September 2001; accepted for publication 4 April 2002)

Scanning Kelvin probe microscopy is used to image surface potential variations in GaN (0001) grown by hydride vapor phase epitaxy. The influence of finite probe tip size on these measurements is analyzed, suggesting that significant differences between measured and actual surface potential variations may exist. Experimentally, localized regions in which the surface work function increases by ~0.1–0.2 V are observed, indicating a shift in the Fermi level toward the valence band; these are attributed to the presence of negatively charged threading dislocations. The magnitudes of the observed variations in surface potential are comparable to those reported in the literature, and compare favorably with those predicted on the basis of a model in which the dislocation is represented as a filled line of acceptor states and the interaction between the sample and a probe tip of finite size is considered. In this model, the finite size of the probe tip is found to exert a substantial influence on the degree to which the full variation in surface potential is observed in scanning Kelvin probe measurements. © *2002 American Institute of Physics.*
[DOI: 10.1063/1.1481208]

I. INTRODUCTION

The scarcity of large-area, high-quality homoepitaxial substrates for growth of GaN films by molecular-beam epitaxy (MBE) or metalorganic chemical vapor deposition (MOCVD) typically results in the presence of high concentrations of threading dislocation lines in epitaxially grown nitride semiconductor material. Various types of threading dislocations can degrade device performance via Coulomb scattering arising from charged acceptor states,[1,2] increased nonradiative recombination,[3,4] and creation of vertical current leakage paths.[5,6] Hydride vapor phase epitaxy (HVPE) may offer an economically attractive method for the preparation of free-standing GaN substrates of thick, low-dislocation-density GaN-layers for use as templates for epitaxial growth: high HVPE growth rates (~1 μm/min) at or near equilibrium conditions result in films exhibiting dislocation densities that decrease substantially with increasing film thickness, from greater than 10^9 cm^{-2} in very thin films to $\sim 5\times 10^7$ cm^{-2} for films ~40 μm or greater in thickness.[7,8] A detailed understanding of the electronic properties of the surface and of defects such as threading dislocations is, however, necessary if HVPE-grown material is to be used as a template for subsequent nitride growth by MBE or MOCVD.

In this paper, we describe imaging and analysis, using scanning Kelvin probe microscopy (SKPM), of the nature and spatial distribution of surface potential variations present in GaN films grown by HVPE. Scanning Kelvin probe microscopy images of GaN films ranging in thickness from 0.5 to 14 μm reveal localized variations in surface potential with typical amplitudes of ~0.1–0.2 V. The spatial distribution of the observed surface potential variations changes considerably with increasing GaN layer thickness, in a manner consistent with decreasing threading dislocation density at the film surface. Furthermore, a detailed analysis of the change in surface potential one would expect to measure in the vicinity of a charged threading dislocation, accounting for both the potential arising from the charged dislocation and the finite probe tip size, reveals that the observed surface potential shift is, for realistic tip sizes, considerably smaller than the actual shift in the immediate vicinity of the dislocation core. This conclusion is expected to be applicable for SKPM imaging of any highly localized surface potential variation.

II. EXPERIMENT

Three GaN samples, with GaN layer thicknesses of 0.5, 1.1, and 14 μm, were grown by HVPE on ZnO buffer layers on sapphire substrates. Details of the growth conditions and procedures have been presented elsewhere.[8] Previous studies by transmission electron microscopy have indicated that dislocation densities of $\sim 10^{10}$ cm^{-2} are present near the interface between the GaN and buffer layers, decreasing to $\sim 3\times 10^8$ cm^{-2} at the GaN surface after ~20 μm of film growth.[9] Transport studies have indicated that *n*-type carrier concentrations of $\sim 5\times 10^{19}$ cm^{-3} are present near the substrate-film interface, decreasing to $\sim 10^{17}$ cm^{-3} near the film surface.[10] All samples used in our studies were cleaned initially with trichloroethylene, acetone, and methanol in an

[a)]Electronic mail: ety@ece.ucsd.edu

 © 2002 American Institute of Physics

Downloaded 09 Jul 2002 to 132.239.19.110. Redistribution subject to AIP license or copyright, see http://ojps.aip.org/japo/japcr.jsp

ultrasonic bath. Ohmic contacts were fabricated by deposition of Al/Ti metallization and subsequent annealing in N_2 at 650 °C.

Atomic force microscopy (AFM) and SKPM data were obtained in a Digital Instruments Nanoscope® IIIa MultiMode™ unit using Co/Cr-coated tips under ambient conditions. To acquire AFM and SKPM images, a topographic line scan is first obtained by AFM using TappingMode™ imaging, and then that same line is rescanned in LiftMode™ with the tip raised to a lift height typically of ~30 nm.

The basic principles of SKPM have been described in detail elsewhere.[11,12] In brief, SKPM is used to image variations in the surface contact potential difference, $\Delta\phi$ between a conducting probe tip and the sample under investigation and is defined[13] as $\Delta\phi=(\phi_{\mathrm{tip}}-\phi_{\mathrm{GaN}})/q$, where ϕ_{tip} and ϕ_{GaN} are the work functions of the tip and sample surface, respectively, and q is the magnitude of the electron charge. A bias voltage $V_{\mathrm{sample}}=V_{\mathrm{dc}}+V_{\mathrm{ac}}\sin\omega t$ is applied directly to the sample, holding the tip at ground potential. This results in a total electrostatic force F,[14] with a spectral component F_ω at frequency ω, and resonant oscillation amplitude A,[11] given by

$$F=\frac{1}{2}\frac{dC}{dz}[-V_{\mathrm{sample}}-\Delta\phi]^2, \tag{1a}$$

$$F_\omega=-\frac{dC}{dz}[(-V_{\mathrm{dc}}-\Delta\phi)V_{\mathrm{ac}}\sin\omega t], \tag{1b}$$

$$A=\pi\varepsilon_0 V_{\mathrm{ac}}(-V_{dc}-\Delta\phi)\left(\frac{Qr}{kz}\right), \tag{2}$$

where C is the capacitance between the tip and sample, z the tip-sample separation, ω the tip resonant frequency, Q the tip quality factor, r the tip radius, and k the cantilever spring constant. The negative sign in front of V_{sample} in Eq. (1a) originates from the fact that we apply bias to the sample while grounding the tip. In the scanning Kelvin probe mode of operation, a feedback loop adjusts and records V_{dc} at each point in a scan to minimize the oscillation amplitude. This recorded V_{dc} is then equal, but opposite in sign, to the contact potential difference $\Delta\phi$, since A, and therefore F_ω, is minimized at $V_{\mathrm{dc}}=-\Delta\phi$.[15,16]

III. RESULTS AND DISCUSSION

Figure 1 shows AFM topographic and SKPM surface potential images for each of the three samples studied. The topographic images reveal surface depressions with typical diameters of approximately 100 nm at densities of $\sim10^6$ cm^{-2} in the 0.5 and 1.1 μm samples, with virtually none present in the 14 μm sample. Pinned step edges, which typically indicate the presence of either pure screw or mixed dislocations,[17,18] are visible in abundance in topographic images of all three samples.

The SKPM images shown in Fig. 1 reveal that lateral surface contact potential variations of 0.1–0.2 V are present in all three samples. Bright regions in the SKPM image indicate regions of the sample with higher work function, i.e., those regions in which the Fermi level is closer to the valence-band edge. However, the characteristic lateral length

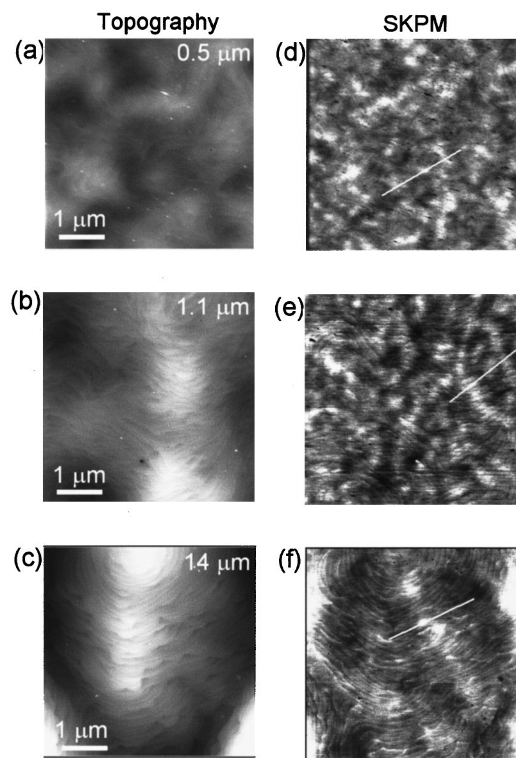

FIG. 1. AFM topographs and surface potential images of GaN films 0.5, 1.1, and 14 μm in thickness. The gray scales correspond to a range of 15 nm for the AFM topographs (a)–(c) and a range of 0.2 V for the surface potential images (d)–(f).

scales over which these variations occur clearly increases with increasing GaN layer thickness. The surface potential contrast patterns observed, particularly in Fig. 1(b), are suggestive of dislocation arrays formed at island coalescence boundaries, such as are commonly found in GaN films grown by a variety of methods on sapphire substrates.[2,19–23] The typical distances we observe between such coalescence boundaries, approximately 0.8–1.6 μm, are consistent with those reported for both HVPE-grown material[24] and MOCVD films.[25] For the 0.5 μm GaN film, we also observe regions at a density of $\sim10^6$ cm^{-2} (not shown), ~100–500 nm in diameter, exhibiting local surface potentials ~0.3–0.4 V lower than the surrounding area. These regions are not associated with surface pits.

Figure 2 shows plots of surface potential variations measured for all three samples along the paths indicated in Fig. 1. As shown in Figs. 1 and 2, a local increase in the GaN work function, indicated by brighter contrast, of approximately 0.1–0.2 V occurs over some, but not all, pinned step edges, i.e., in the vicinity of mixed or screw dislocations. In addition, numerous features are observed corresponding to surface potential variations that are present in the absence of any significant topographic contrast, as has been reported in other recent studies of surface potential variations in GaN epitaxial films.[26] The latter features may be associated with pure edge dislocations, for which distinct features in surface topography may not be observed.[26,27] The observation of a local increase of the work function in the vicinity of a threading dislocation is consistent with the presence of negative

Downloaded 09 Jul 2002 to 132.239.19.110. Redistribution subject to AIP license or copyright, see http://ojps.aip.org/japo/japcr.jsp

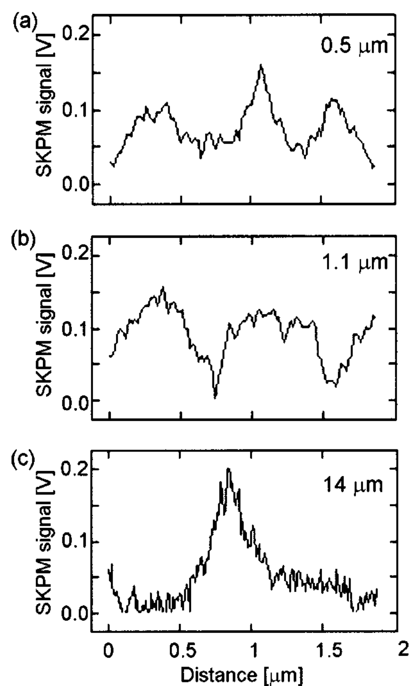

FIG. 2. Surface potential profiles as functions of position for GaN films (a) 0.5, (b) 1.1, and (c) 14 μm in thickness. The profiles shown were extracted along the lines indicated in the corresponding surface potential images in Figs. 1(d)–1(f).

charge in the dislocation core, as has been postulated based on a number of theoretical[28–30] and experimental[2,3,27,31–36] studies of electronic structure associated with and in the vicinity of various types of threading dislocation.

Figures 3(a) and 3(b) show 10×10 μm^2 surface potential images of the 1.1 and 14 μm GaN films, along with two-dimensional power spectra for each image in the insets. Figure 3(c) shows a plot of an averaged radial section through each of the power spectral distributions. As shown in the figure, the characteristic length scale for surface potential variations increases with increasing GaN film thickness, consistent with both a decrease in dislocation density and a decrease in donor concentration at the sample surface as the GaN film thickness increases. Specifically, the average distance between dislocations will increase with decreasing dislocation density, and the range of the surface potential variation associated with each dislocation will increase with decreasing donor concentration. These trends are reflected in the higher intensity of long-wavelength components ($\geqslant 1$ μm) and lower intensity of short-wavelength components ($\leqslant 0.75$ μm) for the 14 μm sample when compared to the 1.1 μm sample.

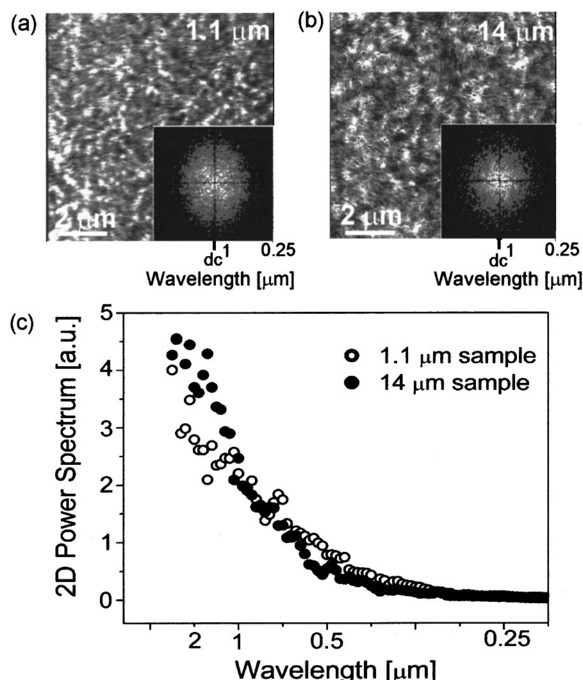

FIG. 3. Surface potential images for GaN films (a) 1.1 and (b) 14 μm in thickness, with two-dimensional power spectrum for each image shown in the insets. (c) Averaged power spectral distributions for the transforms shown.

Further analysis must be informed by the fact that localized surface potential variations measured by SKPM will be influenced by a variety of factors, including the charge distribution associated with the specific defect giving rise to the surface potential feature; screening of a defect-related potential by surface states; and the influence of the measurement technique itself, which may cause the measured value of the variation in surface potential to deviate from the actual value, particularly for highly localized features. An understanding of this last factor is of particular interest in the interpretation of these and related measurements by SKPM of surface potential variations in GaN and other materials.

To assess the influence of the finite size of the probe tip on local surface potential variations measured by SKPM (hereafter referred to as the SKP signal), we have analyzed a simple model of the scanning Kelvin probe measurement in which the force between a sample with a localized surface potential feature and a probe tip of finite size is computed numerically. As described in Sec. II, in scanning Kelvin probe microscopy the dc component of the applied sample voltage is adjusted to minimize the magnitude of the tip-sample force. We have predicted the voltage at which the tip-sample force is minimized with the use of a commercial device simulation software package.[37] The simulated structure consists of a cylindrically symmetric slab of GaN with an Ohmic aluminum back contact. The metallic tip is positioned above the GaN with a tip-sample separation distance set to the value used during our experiment. The precise electronic structure of impurity-free dislocations in GaN is currently unclear;[29,38] however, oxygen defect complexes are predicted to be particularly stable positioned within the edge dislocation core and to create acceptorlike defect states.[29] The double acceptor defect complex (V_{Ga}-O_N), is predicted to generate acceptor states located at $E_{acc}=0.3$, 1, or 1.4 eV above the valence-band maximum energy E_v, depending on the defect complex position within the dislocation core.[29] The dislocation is therefore defined as a cylindrical region located directly below the probe tip, with a radius equal to the *a* lattice spacing of GaN, and an acceptor concentration chosen such that there are two acceptor defect sites per *c* lattice spacing.

Downloaded 09 Jul 2002 to 132.239.19.110. Redistribution subject to AIP license or copyright, see http://ojps.aip.org/japo/japcr.jsp

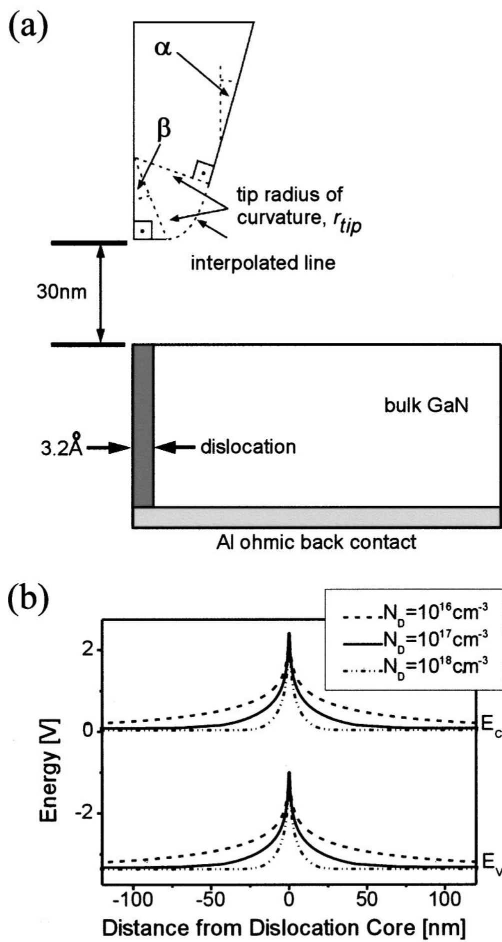

FIG. 4. (a) Schematic diagram of two-dimensional tip and sample geometry with r_{tip}, α, and β tip parameters (not to scale). (b) Simulated band diagrams of the modeled dislocation within bulk GaN showing the effect of bulk GaN dopant density on dislocation-induced potential. The acceptor states located in the dislocation core have an activation energy 1 eV above E_v.

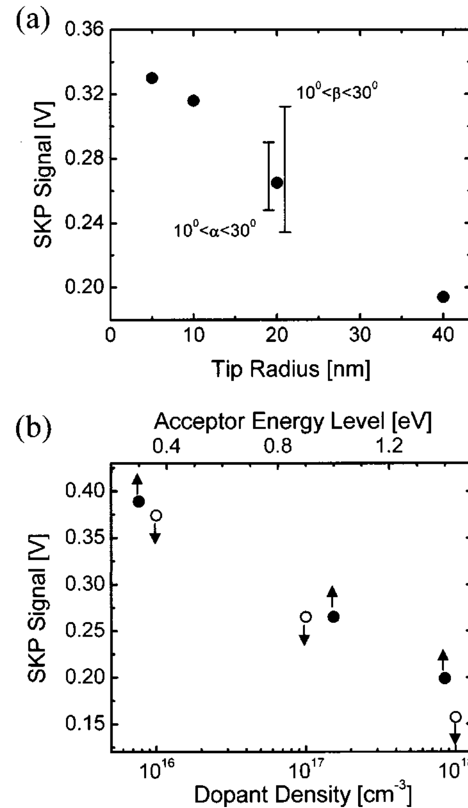

FIG. 5. Simulated *SKP signal due to the presence of a dislocation-induced potential* (a) as a function of tip radius, also showing the effect of varying α and β with $r_{tip}=20$ nm, and (b) as a function of bulk GaN dopant density N_D (open circles) and acceptor activation energy E_{acc} (closed circles). When simulating the effect of varying individual parameters, all other were kept at the nominal values $r_{tip}=20$ nm, $\alpha=20°$, $\beta=20°$, $N_D=10^{17}$ cm^{-3}, and $E_{acc}=1$ eV above the valence-band maximum.

Figure 4(a) shows a two-dimensional schematic of the simulated structure while Fig. 4(b) shows the band edge energy diagram near the modeled dislocation in bulk GaN as a function of bulk GaN dopant density with the double acceptor defect level located 1 eV above E_v. The parameters defining the tip geometry are α, β, and r_{tip}, which represent the tip side angle, tip bluntness, and tip radius, respectively. The two-dimensional structure in Fig. 4(a) is rotated about the center of the dislocation and tip to create a cylindrically symmetric three-dimensional structure. The device simulation software package generates the electric field distribution as a function of sample-tip voltage by numerically solving Poisson's equation at each node of a defined mesh. For each voltage, the electric field distribution is exported and the energy calculated through the volume integration of the electrostatic energy density as shown in Eq. (3). The force F is proportional to the energy gradient[39] according to Eq. (4) and is determined explicitly from energies calculated for tip heights 1 nm above, 1 nm below, and equal to our experimental value:

$$U=\frac{1}{2}\int_V \mathbf{E}\cdot\mathbf{D}\,dV=\pi\int_r\int_Z \varepsilon|\mathbf{E}|^2 r\,dr\,dz, \tag{3}$$

$$F=-\frac{dU}{dz}. \tag{4}$$

The calculated tip-sample force as a function of voltage shows parabolic behavior as a function of V_{dc} as is expected from Eq. (1a). By comparing the values of V_{dc}, at the force minimum, for structures with and without a dislocation, the maximum observed contact potential shift due to the presence of a dislocation, as measured by a probe tip of the modeled dimensions, may be predicted based on Eqs. (1a) and (1b). This observed contact potential shift will be referred to as the SKP signal. Tip geometry (r_{tip}, α, and β) and semiconductor (N_D and E_{acc}) parameters are varied to examine the effect of tip shape and sample properties on the SKP signal.

Figure 5(a) shows a plot of the predicted SKP signal as a function of tip radius and α and β. Each parameter is varied individually while keeping all other parameters fixed at the nominal values $\alpha=20°$, $\beta=20°$, $N_D=1\times10^{17}$ cm^{-3}, and $E_{acc}=1$ eV above E_v. The actual peak value in the work function shift due the presence of the dislocation is approximately 2.4 eV, as shown in Fig. 4(b). However, as shown in Fig. 5(a), the predicted SKP signal is, for reasonable values

Downloaded 09 Jul 2002 to 132.239.19.110. Redistribution subject to AIP license or copyright, see http://ojps.aip.org/japo/japcr.jsp

of tip geometry, expected to be substantially smaller than the actual work function shift at the dislocation core. The tip size influences the magnitude of the SKP signal; this will be the case for any surface potential feature whose size is comparable to or smaller than the tip radius. Also note that as the tip radius increases, the SKP signal decreases. This is reasonable since a probe whose size is much greater than that of the potential feature would be expected to respond only negligibly to the presence of that feature, and, as the tip size becomes much smaller than the potential feature size, the SKP signal should approach the actual peak potential value.

The lines near $r_{tip}=20$ nm in Fig. 5(a) show the effect of varying α and β by 10° above and below their nominal values for r_{tip} fixed at 20 nm. An increase in either α or β decreases the SKP signal. For the tip radius and lift height studied, the tip bluntness β exerts a more significant influence than does α on the SKP signal, although the relative effect of these parameters will likely depend on lift height and the specific potential distribution present on the sample surface. These results are consistent with the trend of larger tips yielding a smaller SKP signal, and the relative importance of the β and α parameters is consistent with simulation results of tip geometry effects on contrast in scanning capacitance microscopy.[40]

Figure 5(b) illustrates the effect of the dopant concentration N_D (open circles) and acceptor energy E_{acc} (closed circles) on the SKP signal. Again, these parameters are varied individually while maintaining all others at the nominal values. N_D was varied by one order of magnitude above and below the nominal value, and the acceptor defect energy levels investigated were 0.3, 1, and 1.4 eV above E_v. Increasing the donor density in the GaN reduces the SKP signal because the spatial extent of the potential is reduced, as shown in Fig. 4(b). The depletion region, induced by the high acceptor trap concentration in the defect, will not extend as far away from the dislocation core with higher N_D. As would be expected, placing the acceptor defect state closer to the valence band increases the SKP signal, although it should be noted that, for the tip and sample parameters investigated, a shift in the defect energy position of 1.1 eV shifts the SKP signal by only 0.18 eV. These results show that detailed tip shape, as well as sample parameters such as dopant concentration, can exert a substantial influence on the observed SKP contrast; however, for the entire range of tip parameters studied, the SKP signal varies by less than a factor of 2 and the measured potential shifts are significantly smaller than true potential shifts.

IV. CONCLUSIONS

We have performed detailed characterization of local surface potential variations in HVPE-grown GaN films using scanning Kelvin probe microscopy, analyzed the dependence of surface electronic structure on GaN film thickness, and assessed the influence of finite tip size on the measurement of highly localized surface potential variations by SKPM. Our measurements have confirmed that, as reported in other studies, surface potential variations typically ~0.1–0.2 V in magnitude are measured on GaN surfaces, and that these variations are associated to a large degree with threading dislocations present at the GaN surface. Further, our measurements demonstrate that the surface electronic structure of HVPE-grown GaN evolves with increasing GaN film thickness to reflect the decrease in threading dislocation density and background donor concentration with increasing GaN film thickness. We have also analyzed the influence of finite tip size on the measurement of highly localized variations in surface potential. Our results demonstrate that the finite size of the probe tip will cause the measured value of a highly localized variation in surface potential to be smaller in magnitude than the actual value, particularly for features that are comparable in size to or smaller than the probe tip radius. These results suggest that the actual surface potential variations in the vicinity of a threading dislocation at the surface of a GaN film may be considerably larger than those measured by us and others using SKPM, and have similar implications for any studies of highly localized features in surface electronic structure using this and related techniques.

ACKNOWLEDGMENTS

Part of this work was supported by ONR Grant Nos. N00014-00-1-0135 (Dr. Colin Wood) and N00014-99-1-0545 (DURIP, Dr. John Zolper).

[1] H. M. Ng, D. Doppalapudi, T. D. Moustakas, N. G. Weimann, and L. F. Eastman, Appl. Phys. Lett. **73**, 821 (1998).
[2] N. G. Weimann, L. F. Eastman, D. Doppalapudi, H. M. Ng, and T. D. Moustakas, J. Appl. Phys. **83**, 3656 (1998).
[3] F. A. Ponce, D. P. Bour, W. Götz, and P. J. Wright, Appl. Phys. Lett. **68**, 57 (1996).
[4] T. Sugahara, H. Sato, M. Hoa, Y. Naoi, S. Kurai, S. Tottori, K. Yamashita, K. Nishino, L. T. Romano, and S. Sakai, Jpn. J. Appl. Phys., Part 2 **37**, L398 (1998).
[5] E. J. Miller, X. Z. Dang, and E. T. Yu, J. Appl. Phys. **88**, 5951 (2000).
[6] J. W. P. Hsu, M. J. Manfra, D. V. Lang, S. Richter, S. N. G. Chu, A. M. Sergent, R. N. Kleiman, L. N. Pfeiffer, and R. J. Molnar, Appl. Phys. Lett. **78**, 1685 (2001).
[7] L. Chernyak, A. Osinsky, G. Noontz, A. Shulte, J. Jasinski, M. Benemara, Z. Liliental-Weber, D. C. Look, and R. J. Molnar, Appl. Phys. Lett. **77**, 2695 (2000).
[8] R. J. Molnar, W. Götz, L. T. Romano, and N. M. Johnson, J. Cryst. Growth **178**, 147 (1997).
[9] Z.-Q. Fang, D. C. Look, J. Jasinski, M. Benemara, Z. Liliental-Weber, and R. J. Molnar, Appl. Phys. Lett. **78**, 332 (2001).
[10] D. C. Look and R. J. Molnar, Appl. Phys. Lett. **70**, 3377 (1997).
[11] M. Nonnenmacher, M. P. O'Boyle, and H. K. Wickramasinghe, Appl. Phys. Lett. **58**, 2921 (1991).
[12] H. O. Jacobs, H. F. Knapp, S. Müller, and A. Stemmer, Ultramicroscopy **69**, 39 (1997).
[13] S. M. Sze, *Physics of Semiconductor Devices*, 2nd ed. (Wiley, New York, 1981), p. 246.
[14] A. K. Henning, T. Hochwitz, J. Slinkman, J. Never, S. Hoffman, P. Kaszuba, and C. Daghlian, J. Appl. Phys. **77**, 1888 (1995).
[15] Support Note No. 231, Rev. A (Digital Instruments, Santa Barbara, CA, 1996).
[16] *Scanning Probe Microscopy and Spectroscopy*, edited by D. Bonnell (Wiley, New York, 2001), p. 218.
[17] F. C. Frank, Discuss. Faraday Soc. **5**, 67 (1949).
[18] D. Kapolnek, X. H. Wu, B. Heying, S. Keller, B. P. Keller, U. K. Mishra, S. P. Denbaars, and J. S. Speck, Appl. Phys. Lett. **67**, 1541 (1995).
[19] L. T. Romano, B. S. Krusor, and R. J. Molnar, Appl. Phys. Lett. **71**, 2283 (1997).
[20] T. Paskova, J. Birch, S. Tungasmita, R. Beccard, M. Heuken, E. B. Sverdberg, P. Tunesson, E. M. Goldys, and B. Monemar, Phys. Status Solidi A **176**, 415 (1999).
[21] X. H. Wu, P. Fini, S. Keller, E. J. Tarsa, B. Heying, U. K. Mishra, S. P. Denbaars, and J. S. Speck, Jpn. J. Appl. Phys., Part 2 **35**, L1648 (1996).

Downloaded 09 Jul 2002 to 132.239.19.110. Redistribution subject to AIP license or copyright, see http://ojps.aip.org/japo/japcr.jsp

[22] T. Araki, Y. Chiba, and Y. Nanishi, J. Cryst. Growth **210**, 162 (2000).
[23] C. Youtsey, L. T. Romano, R. J. Molnar, and I. Adesida, Appl. Phys. Lett. **74**, 3537 (1999).
[24] K. A. Dunn, S. E. Babcock, R. Vaudo, V. Phanse, and J. Redwing, Mater. Res. Soc. Symp. Proc. **482**, 417 (1998).
[25] P. J. Hansen, Y. E. Strausser, A. N. Erickson, E. J. Tarsa, P. Kozodoy, E. G. Brazel, J. P. Ibbetson, U. Mishra, V. Narayanamurti, S. P. Denbaars, and J. S. Speck, Appl. Phys. Lett. **72**, 2247 (1998).
[26] G. Koley and M. G. Spencer, Appl. Phys. Lett. **78**, 2873 (2001).
[27] E. J. Tarsa, B. Heying, X. H. Wu, P. Fini, S. P. Denbaars, and J. S. Speck, J. Appl. Phys. **82**, 5472 (1997).
[28] A. F. Wright and U. Grossner, Appl. Phys. Lett. **73**, 2751 (1998).
[29] J. Elsner, R. Jones, M. I. Heggie, P. K. Stitch, M. Haugk, Th. Frauenheim, S. Öberg, and P. R. Briddon, Phys. Rev. B **58**, 12 571 (1998).
[30] K. Leung, A. F. Wright, and E. B. Stechel, Appl. Phys. Lett. **74**, 2495 (1999).
[31] S. J. Rosner, E. C. Carr, M. J. Ludowise, G. G. Girolami, and H. I. Erikson, Appl. Phys. Lett. **70**, 420 (1997).
[32] C. Youtsey, L. T. Romano, and I. Adesida, Appl. Phys. Lett. **73**, 797 (1998).
[33] P. M. Bridger, Z. Z. Bandic, E. C. Piquette, and T. C. McGill, Appl. Phys. Lett. **73**, 3438 (1998).
[34] B. Heying, E. J. Tarsa, C. R. Elsass, P. Fini, S. P. Denbaars, and J. S. Speck, J. Appl. Phys. **85**, 6470 (1999).
[35] D. M. Schaadt, E. J. Miller, E. T. Yu, and J. M. Redwing, Appl. Phys. Lett. **78**, 88 (2001).
[36] Y. Xin, E. M. James, I. Arslan, S. Sivananthan, N. D. Browning, S. J. Pennycook, F. Omnès, B. Beaumont, J-P. Faurue, and P. Gibart, Appl. Phys. Lett. **76**, 466 (2000).
[37] ATLAS Device Simulator Software, (Silvaco International, Santa Clara, CA, 2000)
[38] J. Elsner, R. Jones, P. K. Sitch, V. D. Porezag, M. Elstner, Th. Frauenheim, M. I. Heggie, S. Öberg, and P. R. Briddon, Phys. Rev. Lett. **79**, 19 (1997).
[39] D. Griffiths, *Introduction to Electrodynamics* (Prentice Hall, Englewood, NJ, 1981), pp. 166–170.
[40] D. M. Schaadt and E. T. Yu, J. Vac. Sci. Technol. B (to be published).

Downloaded 09 Jul 2002 to 132.239.19.110. Redistribution subject to AIP license or copyright, see http://ojps.aip.org/japo/japcr.jsp